Journal of Materials Chemistry A

Accepted Manuscript

ROYAL SOCIETY OF CHEMISTRY

www.rsc.org/materialsA

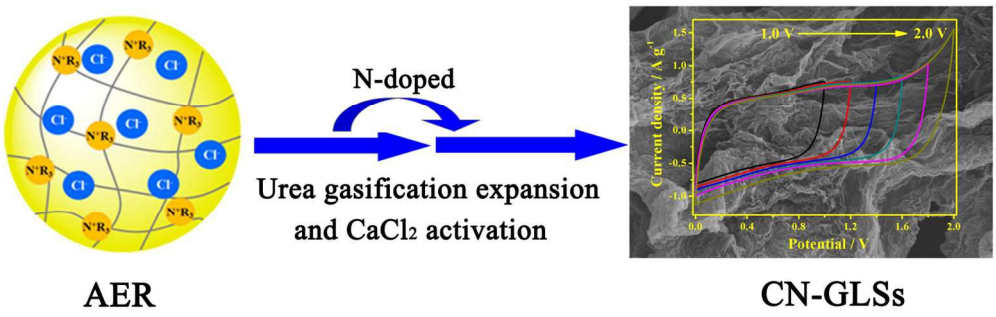

612x196mm (72 x 72 DPI)

Cite this: DOI: 10.1039/c0xx00000x

www.rsc.org/xxxxxx

ARTICLE TYPE

A facile and rapid preparation of highly crumpled nitrogen-doped graphene-like nanosheets toward high-performance supercapacitors

Hui Peng[a], Guofu Ma*[a], Kanjun Sun[b], Zhiguo Zhang[a], Qian Yang[a], Feitian Ran[a] and Ziqiang Lei*[a]

Received (in XXX, XXX) Xth XXXXXXXXX 20XX, Accepted Xth XXXXXXXXX 20XX

DOI: 10.1039/b000000x

Highly crumpled nitrogen-doped graphene-like nanosheets (CN-GLSs) with a high specific surface area (1169 $m^2 g^{-1}$) and large pore volume (2.58 $cm^3 g^{-1}$) is prepared from macroporous resin via simultaneous urea gasification expansion and $CaCl_2$ activation method. The CN-GLSs is tested as electrodes for supercapacitors and presents excellent electrochemical performance.

Two-dimensional (2D) nanomaterials, including the graphene and graphene-like carbon nanosheets, are of great interest as electrode materials in supercapacitors for energy-storage devices, due to its shortened paths for fast electrolyte ion diffusion and large exposed surface offering more electron/charge transfer channels.[1] Furthermore, 2D carbon nanosheets-based supercapacitors will ultimately serve as a low cost, safety and high performance alternative to current commercial conventional activated carbon electric double layer capacitors.[2,3]

A typical 2D planar structure material, graphene, has attracted significant attention in various applications due to its outstanding physicochemical properties.[4] However, graphene nanosheets are apt to form irreversible agglomerates through van der Waals interactions during all phases of graphene preparation and subsequent production procedures,[5] resulting in the deviation of its specific surface area from theoretical values (2630 $m^2 g^{-1}$).[6] Moreover, since the conventional preparation process of graphene is still relatively cumbersome and high cost, this will limit the future industrial application requirements which include easy operation, high yield and high quality. In contrast, 2D porous carbon nanosheets with graphene-like planar structure also have some superior properties possessing less weight, high electrical conductivity and even with larger specific surface area than conventional graphene, which correspond exactly to the requirements for supercapacitors.[7,8] Zheng et al. present a one-step KOH activation of polymerized glucose spheres to prepare porous carbon nanosheets.[9] It exhibits a large surface area (2633 $m^2 g^{-1}$), a high pore volume (1.86 $cm^3 g^{-1}$) and a high rate performance in supercapacitors. Sevilla et al. reported the carbon nanosheets with a thickness of <80 nm is interconnected with a desert rose-like structure that impedes these flat carbon nanoparticles from aggregating and therefore improves the ion diffusion rates.[10] In our previous studies, we introduced one-step activation and N-doping combination method to prepare ultrathin nitrogen-doped carbon nanosheets for high-performance supercapacitors.[11] However, the specific surface area of this material is still less than the ideal (around 550 $m^2 g^{-1}$), due to many large cavities present in the pores. Recently, it is also reported that crumpled sheet morphology can be effective to prevent the face-to-face aggregation of the sheets because of artificial porosity is developed around each layer.[5,12] Thus, it can increase the extensibility and specific surface area of the material. Besides specific surface area and pore geometry, the modification of carbon materials with nitrogen functionalities seems to be the most promising method for enhancing the capacity and surface wettability while maintaining the outstanding cycleability of a supercapacitor.[13] Very recently, various synthesis strategies to fabricate highly crumpled nitrogen-doped graphene or carbon nanosheets are reported, which crumpled sheet morphology is confirmed increases the effective surface area providing excellent capacitive performance, although their specific surface area are still lower than 1000 $m^2 g^{-1}$.[11,14-16] Despite these remarkable achievements, a facile and rapid preparation of highly crumpled nitrogen-doped nanosheets with large specific surface area and high energy density is still challenging. Therefore, to build high-performance carbon-based supercapacitors, the carbon materials should be elaborately designed by taking the morphology and hetero-atomic defects into consideration. The highly crumpled nitrogen-doped graphene-like nanosheets (CN-GLSs) is likely to meet these requirements from the proof-of-concept studies.

In the present work, in order to form 2D CN-GLSs with high specific surface as well as effective nitrogen doping by the simple pyrolysis process, we incorporate urea as a nitrogen source and expansive agent, $CaCl_2$ acts as an activating agent, with macroporous anion exchange resin as carbon source to form a composite to address the above challenges. The synthesized CN-GLSs contains: 1) highly crumpled morphology, which can provide high surface area (1169 $m^2 g^{-1}$) and a large number of exposed active sites, resulting in large capacitance; 2) effective nitrogen doping (about 4.25 wt%) in carbon nanosheets, which exhibits an enhanced pseudocapacitive behavior as well as improves wettability.

The novel CN-GLSs was designed on the basis of the following: i) The macroporous strongly basic quaternary ammonium-type polystyrene-type anion exchange resin (AER) was used as carbon precursor, which contains not only a large amount of quaternary ammonium groups ($(CH_3)_3N$-CH_2-, Fig. 1a) providing a certain amount of nitrogen source, but also the unique macropore structure accommodating nitrogen precursor and activating agent; ii) The urea in the whole system plays a dual

role of nitrogen source and expansive agent;[17] iii) $CaCl_2$ can be seeped into the skeleton of the macroporous AER and acts as an activating agent, then AER was heated to form high surface area and porous carbon nanosheets.[11] A schematic illustration for preparation of CN-GLSs is shown in Fig. 1a. The preparation process mainly consists of two steps: 1) fabrication of carbon precursor mixtures by mixed AER, urea and $CaCl_2$ in ethanol solution under evaporation step. 2) the graphitization and nitrogen-doped process of the carbon precursor to generate 2D highly crumpled nitrogen-doped graphene-like nanosheets (denoted as CN-GLSs) under a N_2 atmosphere by simultaneous urea gasification expansion and $CaCl_2$ activation method. For comparison purposes, only urea mixed with AER or only $CaCl_2$ mixed with AER were carbonized under the same preparation process and the obtained materials were denoted as N-GLSs and C-GLSs, respectively.

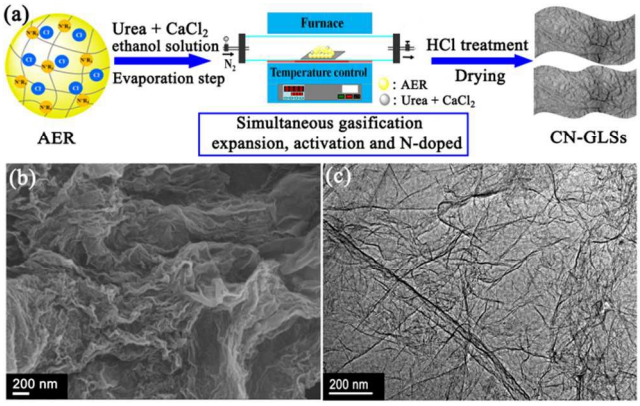

Fig. 1 (a) Schematic of the preparation process of CN-GLSs; (b) SEM images of the CN-GLSs; (c) TEM images of the CN-GLSs.

The morphology and microstructures of the CN-GLSs were characterized by use of scanning electron microscopy (SEM) and transmission electron microscopy (TEM). The CN-GLSs exhibits a fluffy and highly interconnected crumpled structure, which is revealed by typical SEM images (Fig. 1b). In contrast, the N-GLSs prepared by only urea treatment exhibits stacked reticular structure in large lumps (Fig. S1a-b ESI†). Besides, the C-GLSs prepared by only $CaCl_2$ treatment show some crumpled structure (Fig. S1c-d ESI†), but the degree of wrinkles is far lower than the CN-GLSs. Therefore, it is reasonable to infer that the highly interconnected crumpled structure of CN-GLSs is caused by the synergy between urea and $CaCl_2$. This highly crumpled structure was further confirmed by TEM, as shown in Fig. 1c. The CN-GLSs exhibits an ultrathin silk-like morphology with highly interconnected and soft wrinkles. Furthermore, the wrinkles trace of the layer folded each other are clearly visible by high-resolution TEM (Fig. S2 ESI†), indicating that these wrinkles were caused by the crumpling of graphene-like nanosheets. The results also revealed that highly crumpled morphology can effectively prevent the aggregation of the sheets.

In order to more clearly understand carbonization process by the simultaneous used urea treatment and $CaCl_2$ activation, we have carried out X-ray powder diffraction (XRD) to analyze the changes of hybrid materials in the stages before and after carbonization (Fig. S3 ESI†). The XRD pattern confirms the main formation of calcium nitrate urea ($C_4H_{16}N_8O_4{\cdot}Ca(NO_3)_2$, JCPDS no. 44-0719) and caoxite ($Ca(C_2O_4){\cdot}3H_2O$, JCPDS no. 20-0232) after carbonized hybrid samples. Apparently, it is a complex reaction process. The thermal decomposition products of urea are very complicated, containing NH_3, $(HNCO)_x$, biuret, ammeline, ammelide and so on.[17] Therefore, the gas generated by thermally decomposing of urea in this process has multiple functions including nitrogen source and expansion of macroporous AER. Synchronously, $CaCl_2$ activating agent can be seeped into the skeleton of the macroporous AER and heated to form high surface area carbon nanosheets. The representative XRD pattern of the CN-GLSs shows a broad (002) reflection (2θ = 21.7°), and the corresponding interlayer spacing is calculated to be ca. 0.408 nm, a value is larger than that of pristine graphite (0.335 nm). The result suggests that regions of expanded stacking for example through more corrugated or disordered graphene sheets.[18] Unusually, there is a weak peak at 2θ = 11.8°, which may be a result of the channel at the folding axis and similar to the intertube space of multiwalled carbon nanotubes.[19]

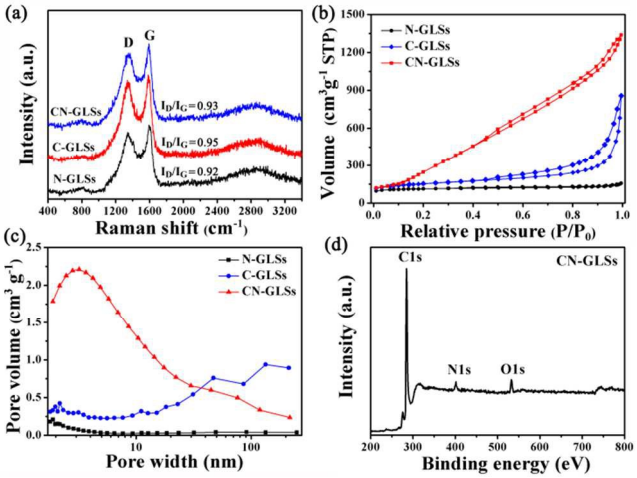

Fig. 2 (a) Raman spectrum of the N-GLSs, C-GLSs and CN-GLSs; (b) Nitrogen adsorption-desorption isotherms and (c) pore size distribution curves of the N-GLSs, C-GLSs and CN-GLSs; (d) X-ray photoelectron spectroscopy (XPS) of CN-GLSs.

The Raman spectrum of all the samples is shown in Fig. 2a. The D-band located at approximately 1340 cm^{-1} corresponds to the defect-induced structure or graphene edges, while the G-band peaked at 1589 cm^{-1} is attributed to amorphous sp^2-bonded forms of carbon.[10] Moreover, the intensity ratio of D-band to G-band (I_D/I_G) for NC-GLSs, C-GLSs and N-GLSs were calculated to be 0.93, 0.95 and 0.92, respectively. These results demonstrate that using $CaCl_2$ activation treatment can promote the formation of the nanosheets with fewer structural defects. The nitrogen adsorption-desorption isotherms of samples prepared under different preparation conditions are displayed in Fig. 2b and categorized as being of type IV, indicating that the porosity is mainly made up of mesoporous. Obviously, the C-GLSs shows a sharp capillary condensation step at high relative pressures (P/P_0 = 0.85-0.99), indicating there existed a relatively large pore size. However, the CN-GLSs shows a slope of the 45° curve increase in the amount of nitrogen-uptakes at relative pressures P/P_0 from 0.45 to 0.99, suggesting the coexistence of mesopores and macropores and it may be constructed from the incompact stacking, entanglement and overlap of carbon nanosheets. The

specific surface area of the CN-GLSs measured by the Brunauer-Emmett-Teller (BET) method is 1169 m^2 g^{-1}.To our surprise, the CN-GLSs shows a total pore volume of up to 2.58 cm^3 g^{-1}, which is much larger than that of N-GLSs and C-GLSs (Table S1 EIS†), and even larger than those mesoporous carbon and the general graphene recently reported.[5,7,20] The corresponding pore size distribution curves of as-prepared samples were obtained from the data evaluation by the Barrett-Joyner-Halenda (BJH) method (Fig. 2c). We can observe that the pore sizes of the CN-GLSs is distributed narrowly and centered in the range of 2-10 nm, suggesting the existence of abundant mesopores. While only the urea gasification expansion or $CaCl_2$ activation was used in the synthesis, both N-GLSs and C-GLSs exhibit relatively low adsorption volume, meaning the low pore volume. Elemental analysis, BET surface area, and pore structure characterization parameters of all samples are summarized in Table S1. The nitrogen contents of CN-GLSs and N-GLSs are greater than 4 wt % and significantly higher than that in C-GLSs (0.91 wt%). The CN-GLSs was further characterized by element mapping images of carbon, oxygen and nitrogen to analyze the elemental distribution (Fig. S4 ESI†). The uniform distribution of green dots (nitrogen) suggests that nitrogen is uniformly doped in the CN-GLSs carbon skeleton. The surface composition of the CN-GLSs sample was studied by XPS (Fig. 2d). There are three peaks at around 284.8, 401.6, and 531.9 eV that correspond to the C 1s, N 1s and the O 1s spectrum, respectively.[11] The bonding configurations of nitrogen atoms are confirmed by high-resolution XPS (Fig. S5 ESI†), and the results show four types of N-containing groups: pyridinic-N (N-6, 398.3 eV), pyrrolic-N (N-5, 400.5 eV), quaternary-N (N-Q, 401.4 eV), and pyridine-N-oxide (N-X, 403.1 eV), respectively.[21] These results further demonstrate that the simultaneous urea gasification expansion and $CaCl_2$ activation methods in combination for the preparation of CN-GLSs can significantly enhance its specific surface area, pore volume and provide effective nitrogen-doping in carbon nanosheets.

To evaluate the advantages of as-prepared materials and their potential applications as electrodes for supercapacitors, the electrochemical performance analyzed of those electrodes were first measured in 6 M aqueous KOH using a three-electrode system. Fig. 3a shows typical cyclic voltammetric (CV) curves of N-GLSs, C-GLSs and CN-GLSs from -1.0 to 0 V at scan rates of 50 mV s^{-1}. The N-GLSs prepared by only urea treatment exhibits a small irregular triangular curve, because the electrolyte ions cannot diffuse easily and thus lead to an ion sieving effect.[22] Conversely, C-GLSs and CN-GLSs show rectangular-shaped CV curves because they have a crumpled and developed porous structure. Obviously, the CN-GLSs has a higher specific capacitance than that of N-GLSs and C-GLSs electrodes due to the linear relation between CV curve area and specific capacitance. Besides, the CV curves of CN-GLSs retain a stable rectangular-like shape even at a scan rate of up to 300 mV s^{-1} (Fig. 3b), suggesting the material exhibits a remarkable rate capability. The galvanostatic charge/discharge measurements were carried out at various current densities ranging from 0.5 to 20 A g^{-1} within the potential window from -1.0 to 0 V, as shown in Fig. 3c. All the curves are highly symmetrical at various current densities, meaning that such electrode possesses excellent electrochemical reversibility properties. The specific capacitances of the electrode materials are calculated from galvanostatic charge/discharge curves according to the equation (Experimental section, ESI†). The correlation between the discharge capacitance and the various current densities for different electrodes are presented in Fig. 3d. In the case of CN-GLSs, the specific capacitance calculated from the galvanostatic discharge curve is up to 294 F g^{-1} at a current density of 0.5 A g^{-1}. When the current density increased to 20 A g^{-1}, the specific capacitance still remains at 226 F g^{-1} with about 78% capacitance retention. These values are significantly higher than that of N-GLSs (211 F g^{-1}) and C-GLSs (180 F g^{-1}) at current density of 0.5 A g^{-1}. The excellent property of CN-GLSs should be attributed to its highly crumpled graphene-like nanostructure and effective nitrogen doping, which provide fast and efficient charge transfer as well as good electrolyte penetration. We compared the capacitance values, BET surface area and pore volume of different crumpled graphene or carbon nanosheets electrode materials previously reported in the literature, as listed in Table S2, ESI.†

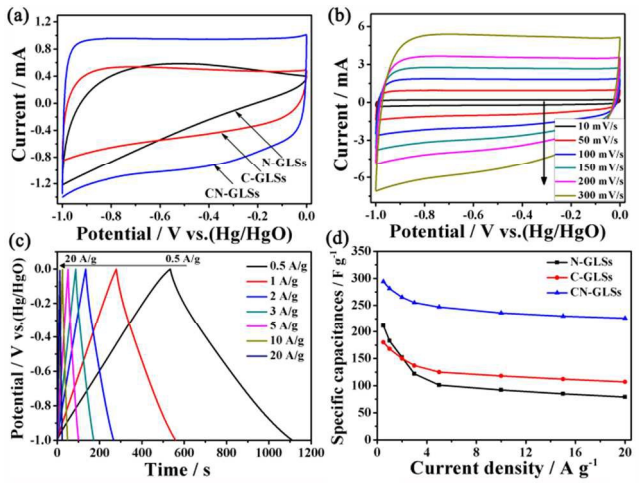

Fig. 3 (a) CV curves of N-GLSs, C-GLSs and CN-GLSs electrodes at a scan rate of 50 mV s^{-1}; (b) CV curves of CN-GLSs electrode at different scan rates; (c) galvanostatic charge/discharge curves of CN-GLSs electrode at various current densities; (d) discharge capacitances of N-GLSs, C-GLSs and CN-GLSs electrodes at various current densities.

For practical applications, the two-electrode symmetric cell was also fabricated in neutral aqueous electrolytes to further investigate the electrochemical performance of the CN-GLSs electrode. It is reported that neutral Na_2SO_4 aqueous electrolyte possesses a higher operation voltage than that in acid and alkali solutions and still prevents the aqueous electrolyte from decomposing.[23,24] Therefore, the CN-GLSs symmetric cell was assembled with 0.5 M Na_2SO_4 aqueous electrolyte. Firstly we need to optimize voltage range and determine the electrochemical stability of device. The as-assembled symmetric cell was measured at different potential windows from 1.0 to 2.0 V at a scan rate of 20 mV s^{-1}, and the resulting CV curves are exhibited in Fig. 4a. The CV curves of the symmetric cell still retain a rectangular-like shaped even when the high voltage extends to 1.8 V, indicating ideal capacitive behavior and good reversibility. However, when the voltage increases to 2.0 V, the current value in high potential increases sharply, which could be caused bythe electrolyte decomposition with hydrogen and/or oxygen

evolution.[23] Therefore, the voltage range of 0-1.8 V was chosen to investigate the overall electrochemical performance of the symmetric cell.

The typical CV curves at different scan rates from 10 to 100 mV s^{-1} are displayed in Fig. 4b. The CV curve areas increas with increasing scan rate, but the shape does not change significantly even at a high scan rate of 100 mV s^{-1}, indicating rapid transportation of electrolyte ions and excellent rate capability. The CV curves of the symmetric cell display slight hump peaks under low scan rates, which can be thought of as Faradaic reactions incurred by N-containing functional groups on the surfaces of the carbon skeleton. As similar to the three-electrode system, the galvanostatic charging curves are almost symmetrical with their discharging counterparts as well as good linear voltage-time profiles (Fig. S6 ESI†), demonstrating a good capacitive performance. The Ragone plot (Fig. 4c) of the supercapacitors calculated from discharging curves at the different currents shows that the highest energy density is 17.0 Wh kg^{-1} at a power density of 225 W kg^{-1} and remains 8.3 Wh kg^{-1} at 4540 W kg^{-1}. The obtained maximum energy density is considerably higher than those of recently reported porous carbon symmetric cells in an aqueous electrolyte, and even comparable with nitrogen-doped graphene or heteroatom-doped carbon symmetric cells.[7,25,26] The details are as listed in Table S3, ESI. †

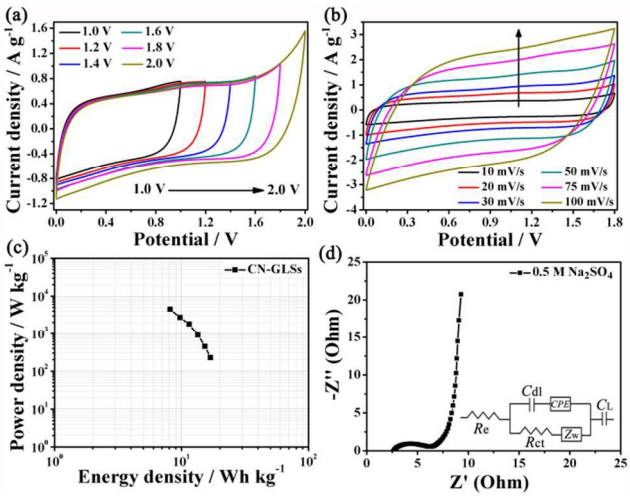

Fig. 4 (a) CV curves of the symmetric cell at different voltage windows. (b) CV curves of the symmetric cell at various scan rates. (c) Ragone plot related to energy and power densities of the symmetric cell. (d) Nyquist plot of the CN-GLSs symmetric cell (the inset of the equivalent circuit).

Fig. 4d shows a Nyquist plot of the CN-GLSs symmetric cell with a small semicircle in the high-frequency region and a vertical curve in the low-frequency region, which indicates a low charge transfer resistance and an excellent capacitive behavior with small diffusion resistance, respectively. The corresponding equivalent circuit from Nyquist plot is as shown in the inset of Fig. 4d, where R_e stands for a combined ohmic resistance of the electrolyte and the internal resistance of the electrode, R_{ct} is the charge transfer resistance caused by the Faradaic reaction. The transition from the semicircle to the long tail of vertical curve is called the Warburg resistance (Z_W) and is a result of the frequency dependence of ion diffusion/transport in the electrolyte to the electrode surface, *CPE* is the constant phase element, C_{dl} is the double-layer capacitance, C_L is the limit capacitance.[24]

According to the equivalent circuit, the CN-GLSs symmetric cell has the low R_e (5.2 Ω cm^2) and possesses a small interfacial R_{ct} (3.1 Ω cm^2). The cycling stability of the CN-GLSs symmetric cell device was tested at a constant current density of 5 A g^{-1} for 5000 cycles (Fig. S7 ESI†). The 97% of the initial capacitance is retained, indicating good long-term stability of the symmetric cell based on the highly crumpled nitrogen-doped carbon nanosheets.

In conclusion, we reported a novel and simple approach to synthesis of 2D interconnected highly crumpled carbon nanosheets. In this way, the graphitization and gasification expansion of the macroporous anion exchange resin and the $CaCl_2$ activation of the carbonaceous material can be integrated into only one step. The as-obtained CN-GLSs shows favorable features for electrochemical energy storage such as graphene-like structures, high specific surface area (1169 m^2 g^{-1}), high pore volume (2.58 cm^3 g^{-1}) and rich nitrogen (4.25%). This novel synthesis route presents a great potential for facile large-scale preparation of highly crumpled nitrogen doping graphene-like nanosheets toward a variety of diverse applications including energy storage, adsorbent, catalyst, and hydrogen storage.

We gratefully acknowledge the financial support from the National Science Foundation of China (Nos. 21164009 and 21174114), the program for Changjiang Scholars and Innovative Research Team in University (IRT1177), Key Laboratory of Eco-Environment-Related Polymer Materials (Northwest Normal University) of Ministry of Education.

Notes and references

[a]*Key Laboratory of Eco-Environment-Related Polymer Materials of Ministry of Education, Key Laboratory of Polymer Materials of Gansu Province, College of Chemistry and Chemical Engineering, Northwest Normal University, Lanzhou 730070, China*
Fax/Tel: +86-931-7975121;
E-mail: magf@nwnu.edu.cn; Leizq@nwnu.edu.cn
[b]*College of Chemistry and Environmental Science, Lanzhou City University, Lanzhou 730070, China*

† Electronic Supplementary Information (ESI) available: Experimental details and electrochemical measurements. Fig. S1-S7 and Tables S1-S3. See DOI: 10.1039/b000000x/

1 M. F. El-Kady, V. Strong, S. Dubin, R. B. Kaner, *Science*, 2012, **335**, 1326.
2 X. Zha, H. Tian, M. Zhu, K. Tian, J. Wang, F. Kang, R. A. Outlaw, *J. Power Sources*, 2009, **194**, 1208.
3 X. Peng, L. Peng, C. Wu, Y. Xie, *Chem. Soc. Rev.*, 2014, **43**, 3303.
4 H. Cong, J. Chen, S. Yu, *Chem. Soc. Rev.*, 2014, **43**, 7295.
5 J. Yan, J. Liu, Z. Fan, T. Wei, L. Zhang, *Carbon*, 2012, **50**, 2179.
6 A. K. Geim, *Science*, 2009, **324**, 1530.
7 L. Sun, C. Tian, M. Li, X. Meng, L. Wang, R. Wang, J. Yin, H. Fu, *J. Mater. Chem. A*, 2013, **1**, 6462.
8 Y. Li, Z. Li, P. Shen, *Adv. Mater.*, 2013, **25**, 2474.
9 X. Zheng, W. Lv, Y. Tao, J. Shao, C. Zhang, D. Liu, J. Luo, D. Wang, Q. Yan, *Chem. Mater.*, 2014, **26**, 6896.
10 M. Sevilla, A. B. Fuertes, *ACS Nano*, 2014, **8**, 5069.
11 H. Peng, G. Ma, K. Sun, J. Mu, Z. Lei, *J. Mater. Chem. A*, 2014, **2**, 17297.
12 X. Han, M. R. Funk, F. Shen, Y. Chen, Y. Li, C. J. Campbell, J. Dai, X. Yang, J. W. Kim, Y. Liao, J. W. Connell, V. Barone, Z. Chen, Y. Lin, L. Hu, *ACS Nano*, 2014, **8**, 8255.
13 Z. Jin, A. Lu, Y. Xu, J. Zhang, W. Li, *Adv. Mater.*, 2014, **26**, 3700.
14 Z. Wen, X. Wang, S. Mao, Z. Bo, H. Kim, S. Cui, G. Lu, X. Feng, J. Chen, *Adv. Mater.*, 2012, **24**, 5610.
15 J. Yan, Y. Xiao, G. Ning, T. Wei, Z. Fan, *RSC Adv.*, 2013, **3**, 2566.

16 S. Yang, X. Song, P. Zhang, L. Gao, *J. Mater. Chem. A*, 2013, **1**, 14162.
17 S. Wakelanda, R. Martineza, J. K. Greyb, C. C. Luhrs, *Carbon*, 2010, **48**, 3463.
18 G. Srinivas, Y. Zhu, R. Piner, N. Skipper, M. Ellerby, R. Ruoff, *Carbon*, 2010, **48**, 630.
19 F. Liu, S. Song, D. Xue, H. Zhang, *Adv. Mater.*, 2012, **24**, 1089.
20 G. Ning, Z. Fan, G. Wang, J. Gao, W. Qian, F. Wei, *Chem. Commun.*, 2011, **47**, 5976.
21 Y. H. Lee, Y. F. Lee, K. H. Chang, C. C. Hu, *Electrochem. Commun.*, 2011, **13**, 50.
22 H. Peng, G. Ma, K. Sun, J. Mu, Z. Zhang, Z. Lei, *ACS Appl. Mater. Interfaces*, 2014, **6**, 20795.
23 Q. Wang, J. Yan, Y. Wang, T. Wei, M. Zhang, X. Jing, Z. Fan, *Carbon*, 2014, **67**, 119.
24 J. Chang, M. Jin, F. Yao, T. H. Kim, V. T. Le, H. Yue, F. Gunes, B. Li, A. Ghosh, S. Xie, Y. H. Lee, *Adv. Funct. Mater.*, 2013, **23**, 5074.
25 M. Li, J. Xue, *J. Phys. Chem. C*, 2014, **118**, 2507.
26 L. Chen, X. Zhang, H. Liang, M. Kong, Q. Guan, P. Chen, Z. Wu, S. Yu, *ACS Nano*, 2012, **6**, 7092.

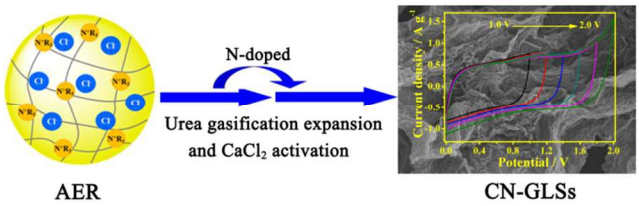

ToC Figure